

Growth of sheets in 3D confinements – a model for the C–S–H meso structure



Merlin A. Etzold^a, Peter J. McDonald^b, Alexander F. Routh^{a,*}

^a BP-Institute, University of Cambridge, Madingley Road, Cambridge CB3 0EZ, UK

^b Department of Physics, University of Surrey, Guildford GU2 7XH, UK

ARTICLE INFO

Article history:

Received 21 February 2014

Accepted 2 May 2014

Available online 21 June 2014

Keywords:

Calcium–silicate–hydrate (C–S–H)

Amorphous material

Hydration products

2D growth

Modelling

ABSTRACT

A numerical model for the growth of amorphous quasi-two-dimensional structures in three-dimensional confinements is presented. Application of this model to the formation of calcium–silicate–hydrates by reaction of anhydrous cement and water, within the interstitial pore space of cement grains, leads to structures with growth and morphological properties consistent with a range of experimental data.

© 2014 Elsevier Ltd. All rights reserved.

1. Introduction

In this work, a phenomenological computer model, which grows amorphous three-dimensional meso-structures from a network of disordered two-dimensional sheets, is introduced. These structure-types are relevant to the morphology of hydrates within cement and the properties of the numerical structures generated are compared to experimental data for cement paste. Such continuum sheet structures are also relevant for other materials such as clays.

The active components of cement are calcium silicate hydrates (C–S–H). C–S–H forms from a dissolution–precipitation reaction of anhydrous cement powder and water. It is related to minerals like tobermorite and jennite [1]. It comprises a disordered network of semi-crystalline layers of calcium and oxygen atoms with silica tetrahedra attached, interspersed by water and further calcium ions. Two water environments are commonly identified: the interlayer water, and water in nanoscopic gel-pores between locally aggregated semi-crystalline layers. The nanostructure has been described as combining glass-like short-range order and features of the mineral tobermorite [2]. However, this model has been criticised for being inconsistent with the crystal chemistry of other calcium silicates [3]. Most macroscopic properties of cement depend on the details of the C–S–H formed. However, the

microscopic morphology of C–S–H remains poorly defined and the subject of intense debate.

For this work, the meso scale is defined as structural features ranging from roughly 1 nm to 500 nm, or, alternatively, bridging the nanoscale with the scale of cement paste. There are two conceptual models [4] of the meso scale morphology of C–S–H. On the one hand are colloidal models such as the recent one due to Jennings [5]. The underlying particle packings of colloidal models have been used to explain a wide range of apparently contradictory experimental results. The colloidal particles have a characteristic length of ca. 5 nm with a layered substructure, where the layers are considered to be chemically similar to those found in minerals like tobermorite and jennite. A hierarchy of nanoscopic pore spaces are identified ranging from the interlayer space, to small pores between disordered layers, between particles in small flocs, and between large flocs [6]. An alternative viewpoint are models such as that due to Feldman and Sereda (FS) [7], which describe C–S–H as quasi-continuous, but disordered, layers of sheets. A schematic contrasting of the models is shown in Fig. 1.

Particle models have received considerable attention from the community. Garrault and Nonat based their model of the formation of hydrated layers on tri- and dicalcium silicate surfaces on particle aggregation [8]. Particle based models have also been used by the group of Ulm to successfully interpret nanoindentation results [9]. Small-angle neutron scattering data of cement paste has been interpreted using fractal particle models [10], finding a mass and a surface fractal and a particle diameter of about 5 nm. Livingston proposed a fractal nucleation and growth model, which successfully relates fit-parameters of

* Corresponding author.

E-mail addresses: merlin@bpi.cam.ac.uk (M.A. Etzold), p.mcdonald@surrey.ac.uk (P.J. McDonald), alex@bpi.cam.ac.uk (A.F. Routh).

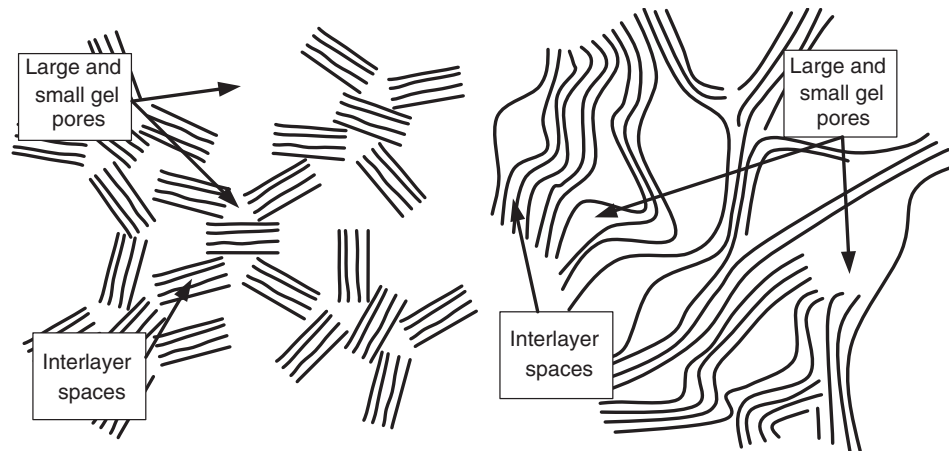


Fig. 1. Schematic of the two dominant C–S–H models: left: the Jennings model is a hierarchical packing of nano-sized layered particles. right: the FS model describes C–S–H as disordered quasi-continuous sheets.

Drawn after [6,7].

the growth rate to the fractal dimensions observed in SANS experiments [11]. This idea is also confirmed by X-ray scattering measurements of Skinner *et al.* They reported a vanishing pair correlation function beyond a correlation length of 3.5 nm and concluded that synthetic C–S–H has nano-crystalline regions of that size. Whilst particle models have been successfully used to fit/explain a broad range of experimental data, difficulties remain in explaining how such structures may form. Ioannidou *et al.* addressed this question with a hybrid Monte-Carlo–molecular-dynamics model, incorporating molecular features below 5 nm to 10 nm by using an experimentally obtained interaction potential. They showed that morphologies observed in micrographs such as fibrils and columns can be formed [12]. Experimentally it is found that localised growth occurs preferentially on the surface of the cement grains [13], instead of cluster formation in the bulk. Recently, Brisard and Levitz studied the relationship between different particle packings and the expected scattering curves. They state that C–S–H cannot be described by monodisperse particle packings and diffusion limited aggregation. They suggest an Apollonian sphere packing with a power-law distribution of particle sizes, or alternatively a power-law distribution of pore sizes [14]. However, recent NMR experiments by Muller *et al.* [15] indicate a rather narrow, bi-modal distribution of pores in C–S–H, consisting of the interlayer and the gel pore space.

Nevertheless, even in the light of the broad success of particle models, doubts remain. Chiang *et al.* developed a fit-model for SANS data based on particles consisting of cylindrical stacks of discs and a fractal pair correlation function. They inferred cylinder heights ranging from 4 nm to 12 nm and diameters between 13 nm and 19 nm for a synthetic C–S–H system equilibrated with different water contents. Such extended sheet regions could also, as they point out, be interpreted as evidence for a quasi-continuous sheet structure [16]. Certainly, this result argues against the idea of 5 nm building blocks. Dolado *et al.* conducted molecular dynamics (MD) simulations of the polymerisation of silicic acid in the presence of water-solvated calcium hydroxide to study “a prejudice-free” structure formation. They observed the formation of a three-dimensional branched structure with building blocks of similar size to Jennings’ particles [4]. They suggest that such a structure may integrate elements similar in size to the colloidal bricks in Jennings’ structure into a continuous structure. Strong phenomenological evidence for the existence of extended sheet-structures can be taken from micrographs of C–S–H both from synthetic systems as well as from cement paste, which often can be described as showing a sheet-like or crumpled-foil morphology [1,17–19]. Brisard *et al.* used transmission X-ray microscopy and associated nanotomography techniques to study cement paste. They showed that the scattering curves can be

related to the nanostructures observed [20]. The images could be interpreted both as a quasi-continuous sheet structure or a colloidal aggregate. McDonald *et al.* used a sheet-model to interpret their NMR results of drying cement paste [21]. Scrivener and Nonat suggested nano-crystalline regions of sheets, partly linked by other sheets, as a C–S–H structure and suggest that such structures may behave mechanically similar to a granular material [22]. Such structures could form according to Gartner by 3D-growth of sheets in space; consequently, this results in a quasi-continuous sheet structure [23]. The ideas proposed by Gartner have never been studied numerically and the resulting material properties of quasi-continuous FS-models have never been investigated in three dimensions due to the difficulty of representing such inherently complex structures.

The literature review above has shown that colloidal models have received considerable attention, and have been successfully applied to interpret experimental data. In contrast, quasi-continuous sheet structures have never been theoretically investigated. In this work, we introduce a methodology to numerically generate three-dimensional amorphous structures that have the core-structural properties of quasi-continuous FS sheet models. These can be tested against experimental results for C–S–H. Initial structures are compared to experimental data obtained with small-angle scattering, isothermal calorimetry, nuclear magnetic resonance (NMR)-porosimetry and permeability data.

2. The sheet growth model

In contrast to the precipitation and aggregation of particles, as modelled by Ioannidou *et al.* [12], this work is based on a different idea. It is assumed that sheet nuclei form instantaneously at time $t = 0$ on the surface of the cement grains, before the acceleration period in the growth. The cement grains dissolve, and C–S–H precipitates at active growth sites on the C–S–H structure. This precipitation is the basis for the model. The motivation for our work is that C–S–H is assumed to be a sheet due to the chemical similarity with tobermorite. This is modelled by assigning the edges of sheets as growth sites. In addition to the planar growth of the sheets, new sheets are assumed to be formed, aligned with existing ones. The modelling idea is similar to the concepts suggested by Gartner [23]. The model adopts a framework to describe arbitrarily shaped surfaces in space based on triangulation. A kinetic sheet growth model with the following seven key elements, based on the hypotheses given above for cement, is implemented within the framework, as shown in Fig. 2. Time evolves in steps of length t_s .

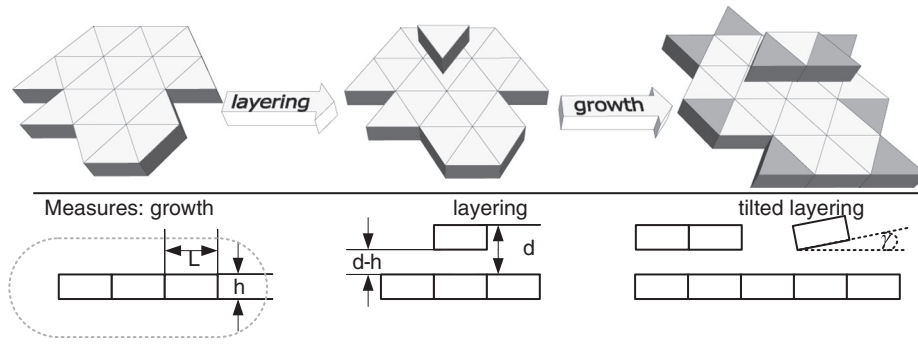


Fig. 2. Top: A new triangle is inserted above a layer during *layering*, and at a layer edge during *growth*. Below: definitions of the geometric measures of the model; a tilting event is also illustrated in two dimensions. The dotted grey line illustrates the exclusion zone.

1. Sheets of thickness h grow within a confined space. Outside of this space, sheets cannot grow.
2. Growth starts from a fixed number of initial nucleation sites N . Nucleation sites are modelled as randomly oriented triangles (prisms) placed on the surface of the confinement space.
3. Planar growth is modelled by adding material to the perimeter of an existing sheet. The probability that a new triangle will be added to an arbitrary perimeter segment during a time step t_s is p_p .
4. Layer formation occurs by inserting a triangle a distance d from existing sheets with a probability p_l during a time step t_s .
5. The pore space sandwiched between aligned layers is called the *interlayer space* and is of width $d_{il} = d - h$. It is formed both by layering and growth from previous layering sites.
6. Sheets are not allowed to intersect. Sheets are surrounded by an exclusion zone, which is sketched in Fig. 2. It prevents triangles from different sheets to be closer than the layer repeat distance d and prevents growth in the interlayer space.
7. Defects in the structures occur due to the exclusion zone and the triangle side length when sheets collide. Additionally, random tilting of new triangles during layering events by an angle γ with a probability of p_t allows control of the number of defects.

In the context of this work, the model is used to simulate the formation of C–S–H in the water-filled capillary pore space between

cement grains. Thus, we model the formation of the C–S–H described by some authors as the outer product [1]. For the time being, we ignore the formation of the inner product and the shrinkage of the cement grains as they are consumed. The capillary space is modelled as a spherical confinement of radius $R_c = 100$ nm, but provisions have been made to also study more complex confinements, as discussed below. The triangle side length, L , is 1.5 nm. The layer repeat distance, d , was chosen as 1.4 nm to fit tobermorite-14 [1,24]. The sheet height was estimated as $h = 0.65$ nm on the basis of crystallographic data for tobermorite-14 [24]. The number of initial seeds, N , was arbitrarily chosen as 500 and will be discussed in Section 4. The tilt angle was chosen as $\gamma = 11^\circ$ on the basis that this leads to wedge-shaped defect pores, analogous to gel pores, with a length-to-thickness ratio of about five, as suggested by NMR data [21].

The algorithm was implemented in Java. After initialisation, the structure is evolved until no further growth is possible. Intermediate structures are described via a progress variable ξ , defined as the number of deposited triangles at time t expressed as a fraction of the total number deposited, N_{Δ}^{final} . The progress variable is analogous to the degree of hydration of cement. Consequently, the time-derivative of ξ is analogous to the reaction rate measured as a heat-flux in isothermal calorimetry or as a volume-change rate in chemical shrinkage experiments.

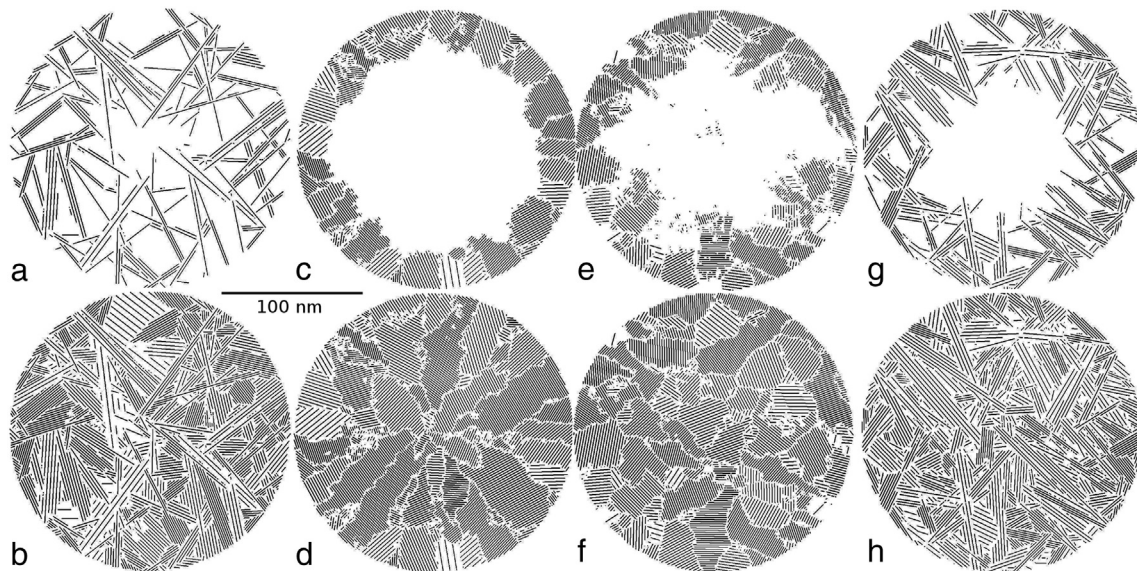


Fig. 3. Example structures generated with the sheet growth algorithm. Shown are situations with different growth parameters. (a) $p_p/p_l = 10^4 \gg 1$. The cavity is rapidly filled by a loose sheet structure which densifies as the structure develops, (b). (c) $p_p/p_l = 1$. A shell of sheets is rapidly formed at the surface of the cavity. Space is filled radially, (d). (e) $p_p/p_l = 10^{-4} \ll 1$. Stacks of sheets form columns growing into the cavity. With time, the stacks expand and fill the space (f). (g, h) $p_p/p_l = 10^3$, $p_t = 0.2$, $\gamma = 11^\circ$. The introduction of tilt is demonstrated. (g) shows an intermediate structure. Note the denser intermediate structure due to the smaller p_p/p_l ratio compared to (a). Structure (h) is the fully evolved structure. This structure is more disordered than structures without tilt. The tilt probability was deliberately chosen to obtain a structure with a ϕ_{il}/ϕ_d fitting Muller's *et al.* NMR results [15].

3. Results

3.1. Growth morphologies

Fig. 3 shows cross-sections through three-dimensional structures grown with different model parameters. Only in the fourth column are sheets allowed to tilt during nucleation. The top row is composed of intermediate structures; the bottom row is composed of the final structures. In the first column, planar growth dominates layering ($p_p \gg p_l$). The space is rapidly filled with an open network of sheets, seen in cross section in the figure. Only as the structure evolves, do the open spaces between the sheets fill in. In the second column, growth and layering are balanced ($p_p = p_l$). This leads to the rapid formation of a dense solid layer covering the confinement surface, the thickness of which grows radially. In the third column, layering dominates growth ($p_p \ll p_l$). Stacks of sheets form rapidly in a needle-like fashion. The tips of some are seen in the centre of the cavity. Again as the system evolves, the spaces between sheets fill in. The three different growth regimes show that strongly anisotropic growth ($p_p \neq p_l$) leads to two-staged space filling. An open structure forms first and then densifies. In contrast, more isotropic growth ($p_p \approx p_l$) leads to the formation of a more uniform layer. Densification of C–S–H during hydration has been measured experimentally by NMR [15]. In the fourth column, Fig. 3g and h, the effect of tilting sheets is demonstrated for growth parameters similar to the first column. The resultant structure is less ordered and less dense. More defects and, hence, more gel pores are formed. Fig. 3b and h are similar to the micrograph of Portland cement shown in Fig. 4. Considering the scaling in Fig. 4, the morphology of the micrographs has approximately similarly sized features. However, other micrographs such as Fig. 12 in [17] show coarser features. It should be noted that preliminary results indicate that the feature size in the generated structures depends on the size of the confinement. Finally, the different morphologies seen in columns one and three may be thought analogous to the two distinct morphologies seen in micrographs of cement pastes that are commonly called foil-like and fibrillar C–S–H [1]. However, we note that the sheet orientation in fibrillar micrographs appears orthogonal to that in the simulation. The closing of larger pores as seen in the sequence Fig. 3a–b can mechanically

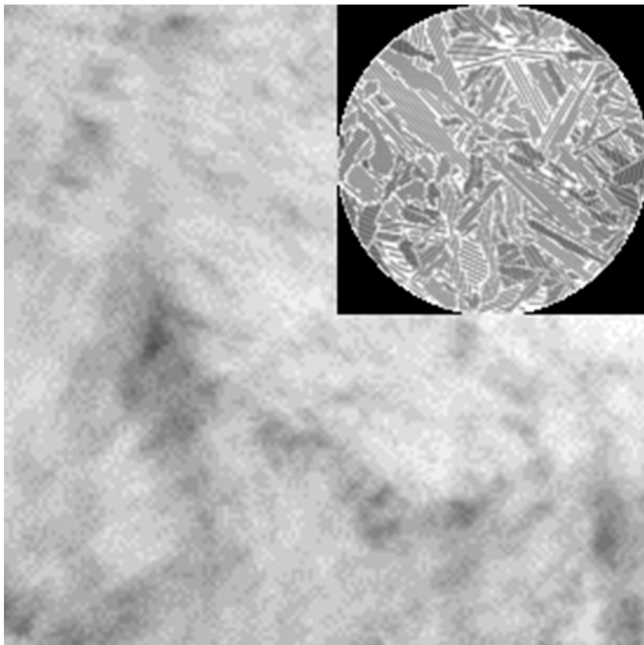


Fig. 4. Micrograph of white Portland cement (400 nm \times 400 nm) and a consistently scaled cross section through a sheet structure. Micrograph by J. Rossen, EPFL.

explain the densification of C–S–H proposed by proposed by Bishnoi and Scrivener from simulations using the modelling platform μic [25].

3.2. Model kinetics

Fig. 5 shows the progress variable and growth rate as a function of time during the evolution of the structure shown in Fig. 3h. The growth rate reaches a maximum after about 350 time steps and a progress variable of roughly 0.4. It shows similarity to the experimentally observed heat flux for the hydration of tricalcium silicate, a major component of commercial cements, which is often used as a model system. An acceleration and deceleration period are observed as seen in hydrating cement paste [26]. This underlines the feasibility of the suggested growth mechanism. However, careful comparison between the curves suggests a shorter deceleration period for the model compared to alite. The structure was grown in a sphere. One criticism of this is that the growth rate is necessarily reduced as material always grows radially inwards in a concave space. The outer product of C–S–H grows between packed, approximately spherical cement grains. Hence, at least in the early stages, it grows into a convexly-bound space. To exemplify the difference, Fig. 5 also shows the growth rate for a structure, with the same parameters, grown in the interstitial space between a cubic array of spheres of radius 100 nm. Only a slight difference is observed for the kinetics curve. The implications of this result from different confinement geometries will be discussed below.

3.3. Model porosity

Table 1 compares the interlayer space volume fraction, ϕ_{il} , the defect or gel porosity ϕ_d , and the surface-to-volume ratios of the two pore types for each of the evolved structures in Fig. 3 with values calculated from published pore sizes and water volume fractions in a white Portland cement measured by NMR [28]. For converting water mass fractions into volume fractions, a water density of 1 g/cm³ was assumed. Good agreement is seen between the surface-to-volume ratios of the two pore volumes in the tilted structure compared to those in the experiment. Moreover, the ratio ϕ_d/ϕ_{il} is in good agreement with the experiment, as are the absolute numbers. This demonstrates how the space distribution between the defect (gel) and interlayer porosity can be tuned using the tilt-probability. The detailed porosities and the surface-to-volume ratios of the model depend on the sheet height h and the layer repeat distance d .

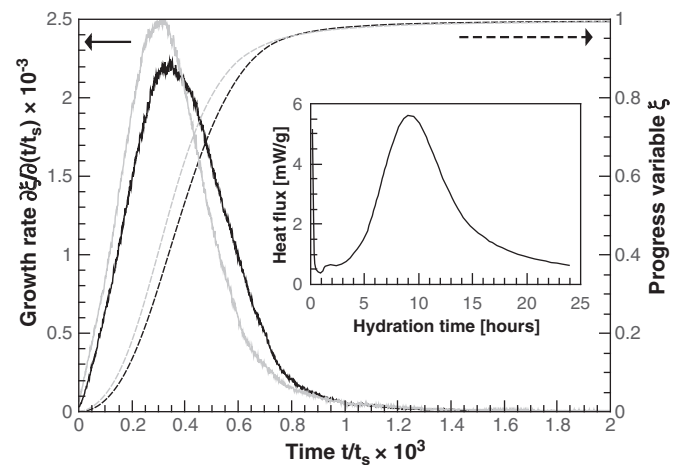


Fig. 5. Black lines: progress variable (dashed) and growth rate (solid) for the structure shown in Fig. 3g and h. Grey lines: the same but for a structure grown between a cubic array of spheres. The inset (reproduced from [27]) shows experimental data for tricalcium silicate paste with a monomodal particle size.

Table 1

Volume fractions (ϕ) and surface-to-volume (S/V) ratios of interlayer (il) and defect (d) pore spaces of the structures shown in Fig. 3 and of a white cement paste calculated from NMR experimental data.

	Fig. 3b	Fig. 3d	Fig. 3f	Fig. 3h	NMR [28]
p_p/p_l	10^4	1	10^{-4}	10^3	n/a
ϕ_{il}	0.27	0.39	0.40	0.24	0.27
ϕ_d	0.37	0.23	0.21	0.42	0.47
S_{il}/V_{il} [nm^{-1}]	2.67	2.67	2.67	2.67	2.13
S_d/V_d [nm^{-1}]	0.94	0.56	0.47	0.97	0.65

3.4. Scattering

Cement morphologies have been investigated by small-angle scattering. The scattering pattern can be simulated by computing the power spectrum of the three-dimensional Fourier transform of the scattering length distribution within the structure [29]. This has been done explicitly by summation of the scattering contribution for every triangle. A powder average was computed by averaging over 200 orientations. In this first study, the removal of domain size effects was not considered as discussed, for example, by Brisard and Levitz [14]. Nevertheless, the interfacial region between the outer product and the inner product/cement grain is not an artefact because it is certainly also seen by experimental small-angle scattering. Fig. 6 shows the calculated scattering pattern for the tilted structure together with the pattern, for the same structure, assuming no contrast between the solid and interlayer space. The former is the scattering from the entire pore surface area whereas the latter is scattering from the gel pore surfaces only. Both curves show identical fringes for small q -vectors, which correspond to the form factor of the spherical confinement. This is demonstrated by the bottom curve in Fig. 6 which is the analytic pattern of a solid sphere [29] with a radius of 100 nm. The first simulation exhibits a distinct peak at 4.467 nm^{-1} , which is not seen in the second. This corresponds to the interlayer spacing d . The peaks at higher q -values are its overtones. For large q -vectors, both curves show a q^{-4} dependence which corresponds to the experimental Porod regime. The simulated data is compared to experimental small-angle neutron scattering data for cement from Allen *et al.* (dashed) [30]. For large and intermediate scattering vectors, and in the case of no contrast between solid and interlayer water, the curves are in general agreement. For small scattering vectors, the form factor of the confinement is seen in simulation. In experiments, the spaces between cement particles are highly irregular in size and shape, so any confinement contribution would be smeared out. As can be seen in Fig. 6, for $q < 0.4 \text{ nm}^{-1}$, the slope of the experimental curve is

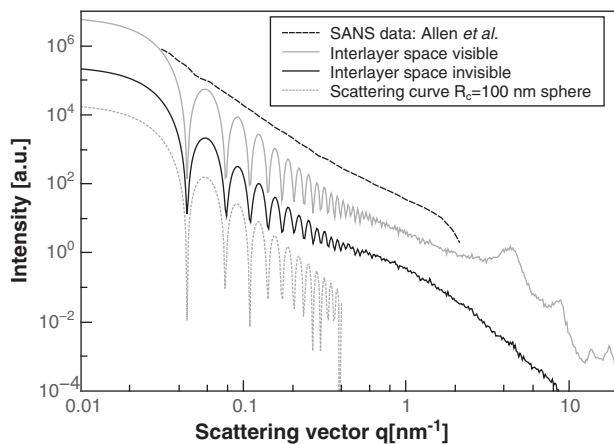


Fig. 6. Example scattering curves obtained for structure (h) in Fig. 3 together with small-angle neutron scattering literature data taken from Allen *et al.* [30]. For clarity, each curve is offset from the next by an intensity factor of 10. From top: the experimental data and then simulated scattering of the tilted structure; the structure without solid–interlayer contrast and the spherical confinement.

slightly less steep than in the simulations. This is interpreted as the surface fractal property of the C–S–H nanostructure [30,31]. The simulation domains are not sufficiently large to verify this.

3.5. Permeability

A standard single-relaxation time lattice Boltzmann permeability scheme has been implemented to calculate the permeability of the structure with and without flow through the interlayer space. The structure was grown within a cylinder with diameter and length of 50 nm and with 31 seeds placed on the surface, using the kinetic parameters of the structure shown in Fig. 3h. The results yield a permeability of $1.4 \cdot 10^{-20} \text{ m}^2$ with fluid flow enabled in all spaces and $1 \cdot 10^{-20} \text{ m}^2$ with flow in the gel spaces only (i.e. no flow in the interlayer). These values suggest that flow through the interlayer is as important as flow through the remaining pore space. Experimental results for the permeability of cement paste vary widely in the range 10^{-18} m^2 to 10^{-22} m^2 , depending on the sample preparation and measurement method [32,33]. The permeability of the C–S–H within the cement is thought to be lower and has been estimated as $7 \cdot 10^{-23} \text{ m}^2$ [34], a value which is more than 100 times less than the simulations here. This discrepancy may be due to the spaces at the edges of sheets. In fully evolved structures, these spaces arise from the exclusion zone of neighbouring sheets and create connectivity of the gel porosity. The chemistry, and hence structure, surrounding sheet edges remains uncertain and such connectivity may not be present. Using the well-known Carman–Kozeny equation for a particle packing with a radius of 5 nm, as suggested for colloidal models [5, 30], and a gel porosity of 0.47 as measured by NMR, gives a permeability of $5 \cdot 10^{20} \text{ m}^2$ for a non-hierarchical colloidal model. This result indicates that, even if the new model cannot yet explain the low permeability of cement paste and C–S–H, it is equally as good as the colloidal model. Further exploration is deferred to a future publication.

4. Discussion of the model

In the previous Sections it has been demonstrated that the algorithm leads to structures whose porosity can be matched to NMR porosimetry data and whose morphology, and scattering curves are in general agreement with experimental data. Comparison between the structures generated by the model and real C–S–H systems can be made only if one accepts the following simplifications: in all experimental systems, the cement grain size and shape are expected to be polydisperse, and the confinement size of $\approx 100 \text{ nm}$ can certainly cover only the lower end of the capillary pore space. Furthermore, the structures were grown with a seed density of almost $4000 \mu\text{m}^{-2}$, which is about 400 times larger than that suggested by Fig. 3(a2) in Alizadeh *et al.* [13]. However, to the best of these authors' knowledge, reliable quantitative data about the seed density on cement grains does not exist.

The influence of the initial seed density is twofold: fewer seeds lead to a reduced number of growth sites and, thus, to slower growth. More critically, without the tilt mechanism, each sheet gives rise to a crystalline layered structure. The long-range disorder in the structures modelled in this work is thus generated by the complex interplay of the sheets growing from different seeds. Microscopic evidence, e. g. by Gartner *et al.* or Alizadeh *et al.* [35,13] suggest that open, expanding

structures grow originating from relatively few nuclei. For the model as it is, the high number of seeds is necessary to induce sufficient disorder into the non-tilted systems. Ongoing work indicates that disorder can also be introduced by a tilt mechanism, either during layer formation, as presented here, or during the planar growth step. This can replace the randomness induced by the large number of seeds, so that only few seeds would be required for anisotropic structures. This is currently the primary aim for the further development of the model. The second aspect concerns the seed density and requires refinement of the location of the defect or gel pore space. As shown in Table 1, those structures without tilt exhibit considerable non-interlayer pore space, which is located between stacks of sheets and is caused by the exclusion zone between the sheets. NMR indicates the formation of the gel pore space as the nanostructure develops [15], whilst the porosity located between stacks of sheets only closes as stacks expand.

The confinement shape (see Fig. 5) as well as its size, affect the characteristic points, namely time of peak growth rate and the corresponding progress variable of the growth rate curve. The extension of the model to include a more polydisperse pore space is currently being pursued. However, due to the space filling nature of the algorithm, properties such as the porosity do not depend on the domain shape as long as the domain is considerably larger than the structural features. Whilst the kinetic curve outlines the applicability of the model to hydrating cement paste, its value must be limited to investigations of the growth order, such as that proposed by Gartner [36,23] because the model currently neither includes any reactant transport information nor represents the complex capillary pore space. The model presented in this work is intended to be as simple as possible because parameters, such as the growth rates, are currently unknown. Thus, it was decided against considering further aspects such as introducing a preferred growth direction in plane, as one may expect due to the crystal structure of tobermorite. It is anticipated to extend the model appropriately as soon as such information, like the relative growth rates in tobermorite, become available from other techniques.

5. Conclusion

In this work, an algorithm is presented simulating the growth of amorphous sheet structures in confinements. It has been applied to the formation of C–S–H in hydrating cement paste. Both the evolution and morphology of the simulated structures correspond with a range of experimental observations. The emerging picture is qualitatively consistent. The results suggest that a systematic exploration of the parameter space of the model combined with further development of the branching sequence will lead to structures with properties that quantitatively match experimental systems. We anticipate that this development will allow progress to be made in a better understanding of the nature and formation of cement's hydration products, a debate benefiting from quasi-continuous sheet models in three dimensions.

Acknowledgements

The authors thank John Rossen of EPFL, Switzerland for providing the micrograph in Fig. 4. This research was funded by the European Commission under grant agreement FP7:26448 and the EPSRC under grant agreement EP/H03333/1.

References

- [1] I.G. Richardson, Tobermorite/jennite- and tobermorite/calcium hydroxide-based models for the structure of C–S–H: applicability to hardened pastes of tricalcium silicate, [beta]-dicalcium silicate, portland cement, and blends of portland cement with blast-furnace slag, metakaolin, or silica fume, *Cem. Concr. Res.* 34 (9) (2004) 1733–1777.
- [2] R.J. Pellenq, A. Kushima, R. Shahsavari, K.J. Van Vliet, M.J. Buehler, S. Yip, F.J. Ulm, A realistic molecular model of cement hydrates, *Proc. Natl. Acad. Sci. U.S.A.* 106 (38) (2009) U.S.A.
- [3] I.G. Richardson, The importance of proper crystal-chemical and geometrical reasoning demonstrated using layered single and double hydroxides, *Acta Crystallogr. Sect. B-Struct. Sci.* 69 (2) (2013) 150–162.
- [4] J.S. Dolado, M. Griebel, J. Hamaekers, The nano-branched structure of cementitious calcium–silicate–hydrate gel, *J. Mater. Chem.* 21 (2011) 4445–4449.
- [5] H.M. Jennings, A model for the microstructure of calcium silicate hydrate in cement paste, *Cem. Concr. Res.* 30 (1) (2000) 101–116.
- [6] H.M. Jennings, Refinements to colloid model of C–S–H in cement: CM-II, *Cem. Concr. Res.* 38 (3) (2008) 275–289.
- [7] R.F. Feldman, P.J. Sereda, New model for hydrated Portland cement and its practical implications, *Eng. J. Canada* 53 (8/9) (1970) 53–59.
- [8] S. Garrault, A. Nonat, Hydrated layer formation on tricalcium and dicalcium silicate surfaces: experimental study and numerical simulations, *Langmuir* 17 (2001) 8131–8138.
- [9] E. Masoero, E. Del Gado, R.J.-M. Pellenq, F.-J. Ulm, S. Yip, Nanostructure and nanomechanics of cement: polydisperse colloidal packing, *Phys. Rev. Lett.* 109 (2012) 155503.
- [10] A.J. Allen, J.J. Thomas, Analysis of C–S–H gel and cement paste by small-angle neutron scattering, *Cem. Concr. Res.* 37 (2007) 319–324.
- [11] R.A. Livingston, Fractal nucleation and growth model for the hydration of tricalcium silicate, *Cem. Concr. Res.* 30 (12) (2000) 1853–1860.
- [12] K. Ioannidou, R.J.-M. Pellenq, E. Del Gado, Controlling local packing and growth in calcium–silicate–hydrate gels, *Soft Matter* 10 (2014) 1121–1133.
- [13] R. Alizadeh, L. Raki, J.M. Makar, J.J. Beaudoin, I. Moudrakovski, Hydration of tricalcium silicate in the presence of synthetic calcium–silicate–hydrate, *J. Mater. Chem.* 19 (2009) 7937–7946.
- [14] S. Brisard, P. Levitz, Small-angle scattering of dense, polydisperse granular porous media: computation free of size effects, *Phys. Rev. E* 87 (2013) 013305.
- [15] A.C.A. Muller, K.L. Scrivener, A.M. Gajewicz, P.J. McDonald, Densification of C–S–H measured by ¹H-NMR relaxometry, *J. Phys. Chem. C* 117 (1) (2013) 403–412.
- [16] W.-S. Chian, E. Fratini, P. Baglioni, D. Liu, S.-H. Chen, Microstructure determination of calcium–silicate–hydrate globules by small-angle neutron scattering, *J. Phys. Chem. C* 116 (2012) 5055–5061.
- [17] I.G. Richardson, The nature of the hydration products in hardened cement pastes, *Cem. Concr. Compos.* 22 (2) (2000) 97–113.
- [18] E. Henderson, J. Bailey, Sheet-like structure of calcium silicate hydrates, *J. Mater. Sci.* 23 (2) (1988) 501–508.
- [19] I. Richardson, J. Skibsted, L. Black, R. Kirkpatrick, Characterisation of cement hydrate phases by TEM, NMR and Raman spectroscopy, *Adv. Cem. Res.* 22 (2010) 233–248 (15).
- [20] S. Brisard, R.S. Chae, I. Bihannic, L. Michot, P. Guttman, J. Thieme, G. Schneider, P.J. M. Monteiro, P. Levitz, Morphological quantification of hierarchical geometries by x-ray nano-ct bridges the gap from nano to micro length scales, *Am. Mineral.* 97 (2012) 480–483.
- [21] P.J. McDonald, V. Rodin, A. Valori, Characterisation of intra- and inter-C–S–H gel pore water in white cement based on an analysis of NMR signal amplitudes as a function of water content, *Cem. Concr. Res.* 40 (12) (2010) 1656–1663.
- [22] K.L. Scrivener, A. Nonat, Hydration of cementitious materials, present and future, *Cem. Concr. Res.* 41 (2011) 651–665.
- [23] E.M. Gartner, A proposed mechanism for the growth of C–S–H during the hydration of tricalcium silicate, *Cem. Concr. Res.* 27 (1997) 665–672.
- [24] E. Bonaccorsi, S. Merlino, A.R. Kampf, The crystal structure of tobermorite 14 Å ... (plombierite), a CSH phase, *J. Am. Ceram. Soc.* 88 (3) (2005) 505–512.
- [25] S. Bishnoi, K. Scrivener, Studying nucleation and growth kinetics of alite hydration using ¹³C, *Cem. Concr. Res.* 39 (2009) 849–860.
- [26] J.W. Bullard, H.M. Jennings, R.A. Livingston, A. Nonat, G.W. Scherer, J.S. Schweitzer, K.L. Scrivener, J.J. Thomas, Mechanisms of cement hydration, *Cem. Concr. Res.* 41 (12) (2011) 1208–1223.
- [27] M.M. Costoya Fernandez, Effect of Particle Size on the Hydration Kinetics and Microstructural Development of Tricalcium Silicate, (Ph.D. thesis) EPF Lausanne, 2008.
- [28] A. Muller, K. Scrivener, A. Gajewicz, P.J. McDonald, Use of bench-top NMR to measure the density, composition and desorption isotherm of C–S–H in cement paste, *Microporous Mesoporous Mater.* 178 (2013) 99–103.
- [29] R.-J. Roe, Methods of X-ray and Neutron Scattering in Polymer Science (Topics in Polymer Science), OUP USA, 2000.
- [30] A.J. Allen, J.J. Thomas, H.M. Jennings, Composition and density of nanoscale calcium–silicate–hydrate in cement, *Nat. Mater.* 6 (2007) 311–316.
- [31] D. Winslow, J.M. Bukowski, J.F. Young, The fractal arrangement of hydrated cement paste, *Cem. Concr. Res.* 25 (1) (1995) 147–156.
- [32] W. Vichit-Vadakan, G.W. Scherer, Measuring permeability of rigid materials by a beam-bending method: III, cement paste, *J. Am. Ceram. Soc.* 85 (6) (2002) 1537–1544.
- [33] H.S. Wong, M. Zobel, N.R. Buenfeld, R.W. Zimmerman, Influence of the interfacial transition zone and microcracking on the diffusivity, permeability and sorptivity of cement-based materials after drying, *Mag. Concr. Res.* 61 (2009) 571–589.
- [34] T.C. Powers, L.E. Copeland, J.C. Hayes, H.M. Mann, Permeability of Portland cement paste, *J. Am. Concr. I.* 51 (1955) 285.
- [35] E. Gartner, K. Kurtis, P. Monteiro, Proposed mechanism of C–S–H growth tested by soft X-ray microscopy, *Cem. Concr. Res.* 30 (5) (2000) 817–822.
- [36] E.M. Gartner, J.M. Gaidis, Hydration Mechanisms, I, The American Ceramic Society, Inc., 1989. 95–126 (Ch. 4).